NONLINEAR BURN CONTROL OF ITER'S TWO-TEMPERATURE PLASMAS USING OPTIMAL AND ADAPTIVE ALLOCATION OF ACTUATORS WITH UNCERTAIN DYNAMICS

V. GRABER, E. SCHUSTER
Lehigh University
Bethlehem, Pennsylvania 18015, USA
Email: graber@lehigh.edu

Abstract

ITER will be the first tokamak to sustain a fusion-producing, or burning, plasma. If the plasma temperature were to inadvertently rise in this burning regime, the positive correlation between temperature and the fusion reaction rate could establish a destabilizing positive feedback loop. Careful regulation of the plasma's temperature and density, or burn control, is required to prevent these potentially reactor-damaging thermal excursions, neutralize disturbances and improve performance. In this work, a Lyapunov-based burn controller is designed using a full zero-dimensional nonlinear model. An adaptive estimator manages destabilizing model uncertainties in the plasma confinement properties and the particle recycling conditions (caused by plasma-wall interactions). The controller regulates the plasma density with requests for deuterium and tritium particle injections. In ITER-like plasmas, the fusion-born alpha particles (and neutral beam particles) will primarily heat the plasma electrons, resulting in different electron and ion temperatures in the core. By considering separate response models for the electron and ion energies, the proposed controller can independently regulate the electron and ion temperatures by requesting that different amounts of auxiliary power be delivered to the electrons and ions. To meet the controller's requested virtual control efforts (the electron heating, ion heating, deuterium fueling and tritium fueling), ITER will have access to the following six actuators: an ion cyclotron heating system, an electron cyclotron heating system, two neutral beam heating systems, a D injector that fires 100% D pellets, and a DT injector that fires 10%D-90%T pellets. An optimal control allocation algorithm is developed to map the four requested virtual control efforts to the six actuators. Adaptive estimation is employed to handle uncertainties in the actuator efficiencies and the other actuator-specific parameters. Furthermore, the adaptive allocator is designed to manage uncertain actuator dynamics. The proposed adaptive burn controller and control allocator are evaluated in a simulation study.

1. INTRODUCTION

The regulation of temperature and density in a fusion-producing (burning) plasma in ITER will require the use of burn control algorithms that request the correct amounts of external heating and fueling for equilibrium stabilization. Because the fast ions introduced from neutral beam injection (NBI) and fusion reactions unevenly heat the plasma ion and electron populations [1, 2], the ion and electron temperatures will be uncoupled. In previous work [3], the authors used Lyapunov techniques [4] to design a nonlinear burn controller based on a two-temperature plasma model. This model assumed that the ion and electron temperatures were proportional through a constant parameter, and the burn controller regulated both temperatures with one control law for the total auxiliary heating. Complex phenomena, such as the ion-electron temperature relationship, were modeled with some level of uncertainty. Uncertainty is modeled by assuming that certain parameters are unknown to the control scheme. This uncertainty can degrade the control performance. The adaptive estimation scheme presented in [3] was designed to counter this hurtle. This prior work [3] was extended in [5] by basing the controller on a two-temperature model with separate response models for the ion and electron energies. In contrast to [3], this burn controller used two unique stabilizing control laws for the external ion and electron heating. In addition, control laws for the external deuterium and tritium injection rates were used to regulate the plasma density.

A controller's requests for external heating and fueling can be met with various actuators. Future ITER plasmas will be fueled by two pellet injectors. One injector supplies pure deuterium (D) pellets, and the other injector supplies a mixture of deuterium and tritium (T). The tritium concentration in the mixed DT pellets will be nominally 90%, but it can vary during plasma operations [6]. An ion cyclotron (IC) heating system, an electron cyclotron (EC) heating system, and two neutral beam injectors (NBI) will be used for plasma heating in ITER [7]. With six actuators (D pellet injector, DT pellet injector, IC, EC, NBI #1 and NBI #2) and four virtual control efforts requested by the controller (D fueling, T fueling, ion heating and electron heating), a control allocation algorithm can be used to optimally map the virtual control efforts to the available actuators. The mapping between the virtual control efforts and the efforts produced by the actuators (i.e., actuator efforts) is known as the effector model. There is an advantage to managing the actuators with a control allocator instead of including them directly in the design of the burn controller. Because the control allocator is designed separately from the burn controller,

reconfigurations in the set of actuators available for burn control do not require modification of the virtual control laws [8]. This modularity allows the control allocator to be swapped for another without changing controllers. As an example, a scenario could occur where only one NBI is available for burn control in ITER. The other NBI may be needed for objectives outside the scope of burn control. Without changing the controller, ITER operators could exchange a control allocator that considers two neutral beam injectors with a different one that considers only one neutral beam injector.

In this work, the proposed burn controller and control allocator improve upon those presented in prior work [5] in numerous aspects. First, the control allocation algorithm in this work is more computationally efficient. The control allocator in [5] mapped the virtual control efforts for the ion and electron heating to the IC, EC and NBI systems by solving a quadratic program at every time step. This is slower than the dynamic update laws [9] that the control allocator in this work uses for the mapping. Second, unlike the prior work [5], the control allocator in this work considers the plasma fueling and pellet injectors. Third, uncertainty is introduced into the effector model by assuming that various constants in it are unknown. The uncertain constants in the effector model include the actuator efficiency factors, the neutral beam heating fractions for the ions and electrons, and the tritium fraction of the DT fueling pellets. This uncertainty is handled by including an adaptive estimation scheme within the control allocator. In [5], the the nonadaptive allocator was based on an effector model that did not include any uncertainty. Fourth, this work introduces actuator dynamics in the form of actuation lag. Actuation lag results from various sources such as the thermalization delay of neutral beam particles. The effects of the actuators on the plasma were assumed to be instantaneous in prior work [3, 5]. In this work, the actuation lag is considered to be uncertain, and yet another adaptive estimator is employed. Finally, the burn controller that provides requested virtual control efforts to the allocator was modified to consider more uncertainty in the plasma model. The proposed adaptive burn controller estimates the uncertain plasma confinement, the DT recycling and impurity sputtering from plasma-wall interactions [10], and the the alpha-particle heating fractions for the ions and electrons.

This paper is organized as follows. In Section 2, the plasma model is presented. Control objectives are considered in Section 3. The stabilizing controller is synthesized in Section 4. In Section 5, both the effector model and the actuator dynamics are discussed. The control allocator is covered in Section 6. With the simulation study presented in Section 7, the performance of the adaptive controller and allocator is assessed. Conclusions and future work are addressed in Section 8.

2. The Two-Temperature Plasma Model

The presented volume-average model assumes that the ions and electrons have unique temperatures, T_i and T_e, respectively. As a result, the ion and electron energies, E_i and E_e, are governed by separate response models,

$$\dot{E}_i = -\frac{E_i}{\tau_{E,i}} + \phi_\alpha P_\alpha + P_{ei} + P_{aux,i}, \qquad \dot{E}_e = -\frac{E_e}{\tau_{E,e}} + (1-\phi_\alpha)P_\alpha - P_{ei} - P_{br} + P_{oh} + P_{aux,e}, \tag{1}$$

where P_α, P_{br}, P_{oh} and P_{ei} are the alpha particle power from fusion, the bremsstrahlung radiation losses, the ohmic heating and the collisional power exchange between the ions and electrons. The fraction of P_α deposited into the plasma ions is ϕ_α. Energy transport out of the plasma is modeled with confinement times $\tau_{E,i}$ and $\tau_{E,e}$. The controlled heating deposited into the ions and electrons are $P_{aux,i}$ and $P_{aux,e}$. The units of each term are Wm^{-3}.

The ion and electron energies are related to particle densities such that $E = E_i + E_e = \frac{3}{2}(n_D + n_T + n_\alpha + n_I)T_i + \frac{3}{2}n_e T_e$, where n_D, n_T, n_α and n_I are the deuterium, tritium, alpha particle and impurity densities. The assumption of quasi-neutrality demands an equal number of protons and elections in the plasma. Therefore, the electron density is $n_e = n_D + n_T + 2n_\alpha + Z_I n_I$ where Z_I is the average impurity atomic number. The density response models are

$$\dot{n}_D = -\frac{n_D}{\tau_D} - S_\alpha + S_D + S_D^R, \quad \dot{n}_T = -\frac{n_T}{\tau_T} - S_\alpha + S_T + S_T^R, \quad \dot{n}_\alpha = -\frac{n_\alpha}{\tau_\alpha} + S_\alpha, \quad \dot{n}_I = -\frac{n_I}{\tau_I} + S_I^{sp}. \tag{2}$$

Each term is expressed in units of $\mathrm{m}^{-3}\mathrm{s}^{-1}$. The particle confinement times are τ_α, τ_D, τ_T and τ_I. Deuterium and tritium are be injected into the plasma at the controlled rates of S_D and S_T, respectively. The impurity sputtering source due to plasma-wall interactions is given by $S_I^{sp} = f_I^{sp}(n/\tau_I + \dot{n})$, where f_I^{sp} is the sputtering fraction and $n = n_D + n_T + n_\alpha + n_I + n_e$. The wall recycling sources for D and T particle, respectively, are modeled with

$$S_D^R = \frac{1}{1 - f_{ref}(1 - f_{eff})}\left\{ f_{ref}\frac{n_D}{\tau_D} + \left(\frac{n_D}{\tau_D} + \frac{n_T}{\tau_T}\right)(1 - \gamma^{PFC})\left[\frac{(1 - f_{ref}(1 - f_{eff}))R^{eff}}{1 - R^{eff}(1 - f_{eff})} - f_{ref}\right]\right\}, \tag{3}$$

$$S_T^R = \frac{1}{1 - f_{ref}(1 - f_{eff})}\left\{ f_{ref}\frac{n_T}{\tau_T} + \left(\frac{n_D}{\tau_D} + \frac{n_T}{\tau_T}\right)\gamma^{PFC}\left[\frac{(1 - f_{ref}(1 - f_{eff}))R^{eff}}{1 - R^{eff}(1 - f_{eff})} - f_{ref}\right]\right\}, \tag{4}$$

where f_{eff} is the fueling efficiency of recycled particles, f_{ref} is the fraction of escaping particles reflected back into the plasma, R^{eff} is the global recycling coefficient, and γ^{PFC} is the tritium fraction of the recycled particles [10].

The DT fusion reaction rate density is given by $S_\alpha = n_D n_T \langle\sigma\nu\rangle$ where the DT reactivity, $\langle\sigma\nu\rangle$, is

$$\langle\sigma\nu\rangle = C_1\omega\sqrt{\xi/(m_r c^2 T_i^3)}e^{-3\xi}, \quad \xi = (B_G^2/4\omega)^{1/3} \quad \omega = T_i\Big[1 - \frac{T_i(C_2 + T_i(C_4 + T_i C_6))}{1 + T_i(C_3 + T_i(C_5 + T_i C_7))}\Big]^{-1}, \tag{5}$$

where T_i is expressed in keV and B_G, $m_r c^2$ and C_j for $j \in \{1, ..., 7\}$ are constants [11]. Because every reaction creates an alpha particle with $Q_\alpha = 3.52$ MeV of kinetic energy, the alpha particle power is $P_\alpha = Q_\alpha S_\alpha$. In contrast to the DT reactivity, the bremsstrahlung radiation losses and the ohmic heating are determined by the electron temperature. They are given by $P_{br} = 5.5 \times 10^{-37} Z_{eff} n_e^2 \sqrt{T_e}$ and $P_{oh} = 2.8 \times 10^{-9} Z_{eff} I_p^2 a^{-4} T_e^{-3/2}$ where $Z_{eff} = (n_D + n_T + 4n_\alpha + Z_I^2 n_I)/n_e$ is the effective atomic number, I_p is the plasma current, and a is the plasma minor radius. The power that is exchanged between the plasma ions and electrons through collisions is given by

$$P_{ei} = \frac{3}{2} n_e \frac{T_e - T_i}{\tau_{ei}}, \quad \tau_{ei} = \frac{3\pi\sqrt{2\pi}\varepsilon_0^2 T_e^{3/2}}{e^4 m_e^{1/2} \ln\Lambda_e} \sum_{ions} \frac{m_i}{n_i Z_i^2}, \tag{6}$$

where τ_{ei} is the relaxation time [12], $m_e = 9.1096 \times 10^{-31}$kg, $e = 1.622 \times 10^{-19}$C, $\varepsilon_0 = 8.854 \times 10^{-12}$F/m, T_e has units of J, and the natural logarithm is $\Lambda_k = 1.24 \times 10^7 T_k^{3/2}/(n_e^{1/2} Z_{eff}^2)$ for $k \in \{i, e\}$.

The global energy confinement time is determined from the IPB98(y,2) scaling law [13]. The scaling is

$$\tau_E = H\tau_E^{sc} = H \times 0.0562 I_p^{0.93} B_T^{0.15} M^{0.19} R^{1.97} \epsilon^{0.58} \kappa^{0.78} P^{-0.69} V^{-0.69} n_{e19}^{0.41}, \tag{7}$$

where H is the H-factor which depends on quality of the plasma confinement, R is the plasma major radius, B_T is the toroidal magnetic field, $\epsilon = a/R$, κ is the vertical elongation at 95% flux surface, V is the volume of the plasma, n_{e19} is n_e in 10^{19}m^{-3}, and $M = 3\gamma + 2(1 - \gamma)$ [14]. The tritium fraction, γ, is equal to the ratio n_T/n_H where $n_H = n_D + n_T$. The total plasma power, $P = P_{aux,i} + P_{aux,e} - P_{br} + P_\alpha + P_{oh}$, is expressed in MWm^{-3}, The machine parameters I_p, B_T, R, a, κ and V, respectively, have values of 15 MA, 5.3 T, 6.2 m, 2 m, 1.7 and 837 m^3 for ITER [14]. With uncoupled temperatures, ions and electrons have different energy transport rates. Therefore, $\tau_{E,i} = \zeta_i \tau_E$ and $\tau_{E,e} = \zeta_e \tau_E$ where ζ_i and ζ_e are constants. Particle confinement times are similarly proportional to (7) such that $\tau_r = k_r \tau_E$ for $r \in \{\alpha, D, T, I\}$.

Fusion reactions and neutral beam injection heat the plasma through the introduction of fast ions. Initially, these fast ions primarily heat electrons. As their kinetic energy falls due to collisional events, increasingly more of their energy goes into the plasma ions. Only at the critical energy, ε_c, do the fast ions evenly heat the plasma ions and electrons. The ion-heating fraction is denoted ϕ_f for $f \in \{\alpha, nbi\}$ to distinguish between alpha-particle heating and neutral beam heating. In prior work [5], the ion-heating fraction was shown to be

$$\phi_f = \frac{1}{x_0}\Big[\frac{1}{3}\ln\frac{1 - x_0^{1/2} + x_0}{(1 + x_0^{1/2})^2} + \frac{2}{\sqrt{3}}\Big(\tan^{-1}\frac{2x_0^{1/2} - 1}{\sqrt{3}} + \frac{\pi}{6}\Big)\Big], \quad \varepsilon_c = \frac{A_f T_e}{m_e^{1/3} n_e^{2/3}} \sum_{ions} \frac{n_i Z_i^2}{A_i}\Big(\frac{3\sqrt{\pi}\ln\Lambda_i}{4\ln\Lambda_e}\Big)^{\frac{2}{3}}, \tag{8}$$

where $x_0 = \varepsilon_{f_0}/\varepsilon_c$, ε_{f_0} is the initial kinetic energy of the fast ion, A_f for $f \in \{\alpha, nbi\}$ is the atomic mass of the fast ion, and A_i for $i \in \{\alpha, D, T, I\}$ is the atomic mass of the plasma ions [1, 15]. For the alpha particles produced from fusion events, $\varepsilon_{\alpha_0} = Q_\alpha$ and $A_\alpha = 4$. ITER's neutral beam heating system injects 1 MeV deuterium particles into the plasma [16]. Therefore, $\varepsilon_{nbi_0} = 1$ MeV and $A_{nbi} = 2$. For the plasma temperatures and densities considered in this work's simulation study of ITER (Section 7), $\phi_\alpha \approx 15\%$ and $\phi_{nbi} \approx 25\%$.

The following parameters are considered to be constant and uncertain: H, ζ_i, ζ_e, ϕ_α, k_D, k_T, k_α, k_I, f_{eff}, f_{ref}, R^{eff}, γ^{PFC} and f_I^{sp} They are lumped into the nominal uncertainty vector θ_h such that (1) and (2) can be rewritten as

$$\begin{aligned}
\dot{E}_i &= -\theta_{h,1}\frac{E_i}{\tau_E^{sc}} + \theta_{h,3}P_\alpha + P_{ei} + P_{aux,i}, & \dot{n}_D &= -\theta_{h,6}\frac{n_D}{\tau_E^{sc}} + \theta_{h,9}\frac{n_T}{\tau_E^{sc}} - S_\alpha + S_{D,} \\
\dot{E}_e &= -\theta_{h,2}\frac{E_e}{\tau_E^{sc}} + \theta_{h,4}P_\alpha - P_{ei} - P_{br} + P_{oh} + P_{aux,e}, & \dot{n}_T &= -\theta_{h,7}\frac{n_T}{\tau_E^{sc}} + \theta_{h,10}\frac{n_D}{\tau_E^{sc}} - S_\alpha + S_T, \\
\dot{n}_\alpha &= -\theta_{h,5}\frac{n_\alpha}{\tau_E^{sc}} + S_\alpha, & \dot{n}_I &= -\theta_{h,8}\frac{n_I}{\tau_E^{sc}} + \theta_{h,11}\frac{n}{\tau_E^{sc}} + \theta_{h,12}\dot{n},
\end{aligned} \tag{9}$$

where $\theta_{h,i}$ is the i^{th} element of θ_h. The elements of θ_h can be easily inferred from (1), (2), (3), (4) and (9).

3. Burn Control Objectives

The purpose of the high-level controller is to track equilibria defined by (9) at steady-state despite the uncertainty in θ_h. The desired equilibrium values for the six states ($\bar{E}_i$, $\bar{E}_e$, $\bar{n}_\alpha$, $\bar{n}_D$, $\bar{n}_T$, $\bar{n}_I$) and the four virtual control efforts ($\bar{P}_{aux,i}$, $\bar{P}_{aux,e}$, $\bar{S}_D$, $\bar{S}_T$) are determined by solving the system of six equations (9) at steady-state with predefined values for $\bar{E}_i$, $\bar{E}_e$, $\bar{n}$ and $\bar{\gamma}$. The deviations of the states from desired values are denoted as $\tilde{E}_i = E_i - \bar{E}_i$, $\tilde{E}_e = E_e - \bar{E}_e$, $\tilde{n}_\alpha = n_\alpha - \bar{n}_\alpha$, $\tilde{n}_D = n_D - \bar{n}_D$, $\tilde{n}_T = n_T - \bar{n}_T$ and $\tilde{n}_I = n_I - \bar{n}_I$. The control objective is to drive the following system to its equilibrium at the origin (i.e., drive the deviations to zero) despite model uncertainties:

$$
\begin{aligned}
\dot{\tilde{E}}_i &= -\theta_{h,1}\frac{\bar{E}_i+\tilde{E}_i}{\tau_E^{sc}} + \theta_{h,3}P_\alpha + P_{ei} + P_{aux,i}, & \dot{\tilde{n}}_D &= -\theta_{h,6}\frac{\bar{n}_D+\tilde{n}_D}{\tau_E^{sc}} + \theta_{h,9}\frac{\bar{n}_T+\tilde{n}_T}{\tau_E^{sc}} - S_\alpha + S_D,\\
\dot{\tilde{E}}_e &= -\theta_{h,2}\frac{\bar{E}_e+\tilde{E}_e}{\tau_E^{sc}} + \theta_{h,4}P_\alpha - P_{ei} - P_{br} + P_{oh} + P_{aux,e}, & \dot{\tilde{n}}_T &= -\theta_{h,7}\frac{\bar{n}_T+\tilde{n}_T}{\tau_E^{sc}} + \theta_{h,10}\frac{\bar{n}_D+\tilde{n}_D}{\tau_E^{sc}} - S_\alpha + S_T,\\
\dot{\tilde{n}}_\alpha &= -\theta_{h,5}\frac{\bar{n}_\alpha+\tilde{n}_\alpha}{\tau_E^{sc}} + S_\alpha, & \dot{\tilde{n}}_I &= -\theta_{h,8}\frac{\bar{n}_I+\tilde{n}_I}{\tau_E^{sc}} + \theta_{h,11}\frac{\bar{n}+\tilde{n}}{\tau_E^{sc}} + \theta_{h,12}\dot{\tilde{n}}.
\end{aligned}
\tag{10}
$$

4. Adaptive Burn Control Algorithm

Control laws for $P_{aux,i}$, $P_{aux,e}$, S_D and S_T are developed using the following Lyapunov function:

$$
V = k_i^2\tilde{E}_i^2 + k_e^2\tilde{E}_e^2 + k_\gamma^2\tilde{\gamma}^2 + \tilde{n}^2 + \tilde{\theta}_h^T\Gamma_h^{-1}\tilde{\theta}_h \quad \rightarrow \quad \dot{V} = k_i^2\tilde{E}_i\dot{\tilde{E}}_i + k_e^2\tilde{E}_e\dot{\tilde{E}}_e + k_\gamma^2\tilde{\gamma}\dot{\tilde{\gamma}} + \tilde{n}\dot{\tilde{n}} + \tilde{\theta}_h^T\Gamma_h^{-1}\dot{\tilde{\theta}}_h, \tag{11}
$$

where k_i, k_e and k_γ are positive constants, Γ_h is a positive definite matrix, and the time derivative is denoted as $\dot{V}$. The controller's current estimate of nominal (uncertain) θ_h is $\hat{\theta}_h$. The $\tilde{\theta}_h$ vector is the controller's estimation error of θ_h such that $\tilde{\theta}_h = \hat{\theta}_h - \theta_h$. By substituting the expressions for the $\dot{\tilde{E}}_i$, $\dot{\tilde{E}}_e$, $\dot{\tilde{n}}$ and $\dot{\tilde{\gamma}}$ dynamics into $\dot{V}$ and employing the the certainty equivalence principle [17] (assume $\hat{\theta}_h = \theta_h$), the four control laws can be formulated as

$$
P_{aux,i}^{stable} = \hat{\theta}_{h,1}\frac{\bar{E}_i}{\tau_E^{sc}} - \hat{\theta}_{h,3}P_\alpha - P_{ei}, \tag{12}
$$

$$
P_{aux,e}^{stable} = \hat{\theta}_{h,2}\frac{\bar{E}_e}{\tau_E^{sc}} - \hat{\theta}_{h,4}P_\alpha + P_{ei} + P_{br} - P_{oh}, \tag{13}
$$

$$
\begin{aligned}
S_D^{stable} = \frac{1}{2}\Bigg[&3\hat{\theta}_{h,5}\frac{n_\alpha}{\tau_E^{sc}} + 2\hat{\theta}_{h,7}\frac{n_T}{\tau_E^{sc}} + 2\hat{\theta}_{h,6}\frac{n_D}{\tau_E^{sc}} + S_\alpha - 2S_T - (Z_I+1)\Big(-\hat{\theta}_{h,8}\frac{n_I}{\tau_E^{sc}}\Big)\\
&- 2\hat{\theta}_{h,9}\frac{n_T}{\tau_E^{sc}} - 2\hat{\theta}_{h,10}\frac{n_D}{\tau_E^{sc}} - (Z_I+1)\hat{\theta}_{h,11}\frac{n}{\tau_E^{sc}} - (Z_I+1)\hat{\theta}_{h,12}\dot{n} - K_N\tilde{n}\Bigg],
\end{aligned}
\tag{14}
$$

$$
\begin{aligned}
S_T^{stable} = &-K_T\tilde{\gamma} + \hat{\theta}_{h,7}\frac{n_T}{\tau_E^{sc}} + S_\alpha - \hat{\theta}_{h,10}\frac{n_D}{\tau_E^{sc}} + \gamma\Big(\hat{\theta}_{h,5}\frac{3n_\alpha}{2\tau_E^{sc}} - \frac{3}{2}S_\alpha - \frac{(Z_I+1)}{2}\Big(-\hat{\theta}_{h,8}\frac{n_I}{\tau_E^{sc}}\Big)\\
&- \frac{(Z_I+1)}{2}\hat{\theta}_{h,11}\frac{n}{\tau_E^{sc}} - \frac{(Z_I+1)}{2}\hat{\theta}_{h,12}\dot{n} - \frac{K_N\tilde{n}}{2}\Big),
\end{aligned}
\tag{15}
$$

where K_N and K_T are positive constants. The above procedure is shown in detail in prior work [3, 5]. Substitution of (12), (13), (14) and (15) into $\dot{V}$ gives

$$
\begin{aligned}
\dot{V} = &-\frac{k_i^2\tilde{E}_i^2}{\tau_E^{sc}}\theta_{h,1} - \frac{k_e^2\tilde{E}_e^2}{\tau_E^{sc}}\theta_{h,2} + k_i^2\tilde{E}_i\frac{\bar{E}_i}{\tau_E^{sc}}\tilde{\theta}_{h,1} + k_e^2\tilde{E}_e\frac{\bar{E}_e}{\tau_E^{sc}}\tilde{\theta}_{h,2} - k_i^2\tilde{E}_iP_\alpha\tilde{\theta}_{h,3} - k_e^2\tilde{E}_eP_\alpha\tilde{\theta}_{h,4}\\
&+ \Big(2\tilde{n} - \frac{k_\gamma^2\tilde{\gamma}}{n_H}\gamma\Big)\frac{n_D}{\tau_E^{sc}}\tilde{\theta}_{h,6} + \Big(2\tilde{n} - (\gamma-1)\frac{k_\gamma^2\tilde{\gamma}}{n_H}\Big)\frac{n_T}{\tau_E^{sc}}\tilde{\theta}_{h,7} + \Big(\frac{k_\gamma^2\tilde{\gamma}}{n_H}\gamma - 2\tilde{n}\Big)\frac{n_T}{\tau_E^{sc}}\tilde{\theta}_{h,9} + (\gamma-1)\frac{k_\gamma^2\tilde{\gamma}}{n_H}\frac{n_D}{\tau_E^{sc}}\tilde{\theta}_{h,10}\\
&- \tilde{n}(Z_I+1)\frac{n}{\tau_E^{sc}}\tilde{\theta}_{h,11} - (Z_I+1)\tilde{n}\dot{n}\tilde{\theta}_{h,12} + 3\tilde{n}\frac{n_\alpha}{\tau_E^{sc}}\tilde{\theta}_{h,5} + \tilde{n}(Z_I+1)\frac{n_I}{\tau_E^{sc}}\tilde{\theta}_{h,8} + \tilde{\theta}_h^T\Gamma_h^{-1}\dot{\tilde{\theta}}_h.
\end{aligned}
\tag{16}
$$

If all parameters are known ($\tilde{\theta}_h = 0$), the stability condition

$$
\dot{V} = -\frac{k_i^2\tilde{E}_i^2}{\tau_E^{sc}}\theta_{h,1} - \frac{k_e^2\tilde{E}_e^2}{\tau_E^{sc}}\theta_{h,2} - K_T\frac{k_\gamma^2\tilde{\gamma}^2}{n_H} - K_N\tilde{n}^2 \leq 0. \tag{17}
$$

is attained. Since the uncertain parameters are generally unknown ($\hat{\theta}_h \neq \theta_h$), the stability condition (17) does not hold with the control laws alone. Therefore, the control laws are augmented with an adaptive law for θ_h:

$$\dot{\hat{\theta}}_h \approx \dot{\tilde{\theta}}_h = \Gamma_h \begin{bmatrix} -(\bar{E}_i/\tau_E^{sc})k_i^2\tilde{E}_i \\ -(\bar{E}_e/\tau_E^{sc})k_e^2\tilde{E}_e \\ P_\alpha k_i^2\tilde{E}_i \\ P_\alpha k_e^2\tilde{E}_e \\ -3\tilde{n}(n_\alpha/\tau_E^{sc}) \\ -[2\tilde{n} - ((k_\gamma^2\tilde{\gamma}\gamma)/n_H)](n_D/\tau_E^{sc}) \\ -[2\tilde{n} - (\gamma-1)(k_\gamma^2\tilde{\gamma})/n_H](n_T/\tau_E^{sc}) \\ -\tilde{n}(Z_I+1)(n_I/\tau_E^{sc}) \\ -(((k_\gamma^2\tilde{\gamma})/n_H)\gamma - 2\tilde{n})(n_T/\tau_E^{sc}) \\ -(\gamma-1)((k_\gamma^2\tilde{\gamma})/n_H)(n_D/\tau_E^{sc}) \\ \tilde{n}(Z_I+1)(n/\tau_E^{sc}) \\ (Z_I+1)\tilde{n}\dot{n} \end{bmatrix}, \tag{18}$$

The adaptive law (18) reduces (16) to (17). Note that $\dot{\hat{\theta}}_h \approx \dot{\tilde{\theta}}_h$ because changes in the uncertain parameters are considered to be negligible ($\dot{\theta}_h \approx 0$). The adaptive control laws (12), (13), (14), (15) and (18) track the equilibria of the error system (10) despite the uncertainty in the model. The stability of $\tilde{n}_\alpha$ and $\tilde{n}_I$ were proven in prior work [5]. The control laws derived in this section represent the requested virtual control efforts $v_s = [\, P_{aux,i}^{stable} \;\; P_{aux,e}^{stable} \;\; S_D^{stable} \;\; S_T^{stable} \,]^T$. In a modular design, the requested virtual control efforts v_s are sent from the controller to the control allocator. The allocator attempts to achieve v_s using the available actuators. The control efforts actually produced by the actuators are denoted $v = [\, P_{aux,i} \;\; P_{aux,e} \;\; S_D \;\; S_T \,]^T$. The allocator attempts to drive the allocation error $|v_s - v|$ to zero.

5. Effector Model and Actuator Dynamics

For the purposes of burn control of the plasma core, ITER will have access to four external heating systems and two external fueling systems. Respectively, the ion cyclotron (IC) and electron cyclotron (EC) systems deliver powers P_{ic} and P_{ec} directly to the ions and electrons independently. The two neutral beam injection (NBI) systems deliver powers P_{nbi_1} and P_{nbi_2} with ion-heating fraction ϕ_{nbi} and electron-heating fraction $(1-\phi_{nbi})$. At an injection rate of $S_{DT_{pel}}$, the DT injector fires pellets that have a nominal 90% T concentration. This T concentration $\gamma_{DT_{pel}}$ can vary during long pulse operations. Therefore, it is considered to be an unknown in the effector model. The D injector fuels the plasma at an injection rate of $S_{D_{pel}}$ with pellets that have no tritium ($\gamma_{D_{pel}} = 0$). The actuators $u = [\, P_{ic} \;\; P_{ec} \;\; P_{nbi_1} \;\; P_{nbi_2} \;\; S_{D_{pel}} \;\; S_{DT_{pel}} \,]^T$ are mapped to the virtual control efforts $v = [\, P_{aux,i} \;\; P_{aux,e} \;\; S_D \;\; S_T \,]^T = \Phi(u)$ through the effector model:

$$\begin{aligned} P_{aux,i} &= \eta_{ic}P_{ic} + \eta_{nbi_1}\phi_{nbi}P_{nbi_1} + \eta_{nbi_2}\phi_{nbi}P_{nbi_2}, & S_D &= \eta_{DT_{pel}}(1-\gamma_{DT_{pel}})S_{DT_{pel}} + \eta_{D_{pel}}S_{D_{pel}}, \\ P_{aux,e} &= \eta_{ec}P_{ec} + \eta_{nbi_1}(1-\phi_{nbi})P_{nbi_1} + \eta_{nbi_2}(1-\phi_{nbi})P_{nbi_2}, & S_T &= \eta_{DT_{pel}}\gamma_{DT_{pel}}S_{DT_{pel}}, \end{aligned} \tag{19}$$

where η_a for $a \in \{ic,\ ec,\ nbi_1,\ nbi_2,\ D_{pel},\ DT_{pel}\}$ are actuator efficiency factors. These efficiency factors, the DT pellet's T concentration $\gamma_{DT_{pel}}$, and the NBI ion-heating fraction ϕ_{nbi} are considered to be constant and uncertain.

Burn control of ITER will have to overcome actuator delays (e.g., the flight time of fueling pellets traveling through guide tubes). The global plasma response times of the EC, IC, NBI and fueling pellet injection systems could be up to 20 ms, 200 ms, 80 ms and 0.1 s, respectively, for ITER [7]. Therefore, the time between when the actuator command is made by the control scheme and when the actuator efforts (u) influence (v) through the mapping (19) is nonzero. The instantaneous actuator commands are denoted $u_{cmd} = [\, P_{ic}^{cmd} \;\; P_{ec}^{cmd} \;\; P_{nbi_1}^{cmd} \;\; P_{nbi_2}^{cmd} \;\; S_{D_{pel}}^{cmd} \;\; S_{DT_{pel}}^{cmd} \,]^T$, and u is the vector of delayed actuation efforts used in (19). The actuator dynamics are modeled as first-order lag processes:

$$T_{lag}\dot{u} + u = u_{cmd}, \tag{20}$$

where $T_{lag} = \mathrm{diag}(\tau_{ic}^{lag},\ \tau_{ec}^{lag},\ \tau_{nbi}^{lag},\ \tau_{nbi}^{lag},\ \tau_{pel}^{lag},\ \tau_{pel}^{lag})$ is a diagonal matrix whose elements are time constants that represent the lag in actuation. These time constants are considered to be uncertain.

All of the time constants are assumed to be proportional to the aforementioned plasma response times from [7] except for τ_{nbi}^{lag}. The time constant for the NBI actuators is the sum of the plasma response time (~ 80 ms) and the more significant NBI thermalization delay. In the plasma, a NBI ion loses energy, ε_{nbi}, at a rate of

$$\frac{d\varepsilon_{nbi}}{dt} = -B\varepsilon_{nbi} - B\varepsilon_{nbi}(\varepsilon_c/\varepsilon_{nbi})^{3/2} \tag{21}$$

where $B = e^4 n_e m_e^{1/2} Z_{nbi}^2 \ln\Lambda_e / (3\sqrt{2}\pi^{3/2}\varepsilon_0^2 m_{nbi} T_e^{3/2})$ [1, 12]. For ITER, the NBI ion's charge Z_{nbi} and mass m_{nbi} are that of a D ion. The NBI thermalization delay can be found by integrating (21) from zero to the thermalization delay. For the plasma conditions considered in Section 7, the NBI thermalization delay is approximately ~ 0.5 s.

6. Adaptive Control Allocation Algorithm

To make the design of the allocation algorithm [9] easier, the high-level dynamics (1)-(2), the effector model (19), and the actuator dynamics (20) are put into a more generalized form. The high-level dynamics are rewritten as $\dot{x} = f(x) + g(x)v$ where $x = [\,E_i \;\; E_e \;\; n_\alpha \;\; n_D \;\; n_T \;\; n_I\,]^T$. Both $f(x)$ and $g(x)$ are easily inferred (θ_h is incorporated into $f(x)$). The effector model (19) and actuator dynamics (20) are rewritten as

$$v = \Phi(u,\theta_e) = \Phi_{\theta_e}(u)\theta_e, \qquad \dot{u} = f_{\theta_u}(u,u_{cmd})\theta_u, \qquad \theta_u = \left[1/\tau_{ic}^{lag} \quad 1/\tau_{ec}^{lag} \quad 1/\tau_{nbi}^{lag} \quad 1/\tau_{pel}^{lag}\right]^T, \tag{22}$$
$$\theta_e = \left[\eta_{ic} \quad \eta_{nbi_1}\phi_{nbi} \quad \eta_{nbi_2}\phi_{nbi} \quad \eta_{ec} \quad \eta_{nbi_1} \quad \eta_{nbi_2} \quad \eta_{D_{pel}} \quad \eta_{DT_{pel}} \quad \eta_{DT_{pel}}\gamma_{DT_{pel}}\right]^T.$$

The vectors θ_e and θ_u lump together the constant, uncertain parameters. The proposed allocator's estimate of them is denoted $\hat{\theta}_e$ and $\hat{\theta}_u$. The $\Phi(u,\theta_e)$, Φ_{θ_e} and $f_{\theta_u}(u,u_{cmd})$ matrices can be easily inferred from the effector model (19) and the actuator dynamics (20). In this generalized formulation, v is unknown, x and u are measured, and u_{cmd} is the controlled input.

The control allocation algorithm takes the desired virtual control reference v_s as an input from the controller and dynamically computes the desired actuator reference u_d as an output. The desired virtual control reference v_s is the vector of stabilizing controls calculated by the high-level controller from (12)-(15). The goal of the allocation algorithm is to get the actual virtual control efforts v from the effector model (19) to match the reference v_s by dynamically updating reference u_d. The low-level control u_{cmd} will attempt to bring the actual actuator efforts u to the computed value of reference u_d. The reference u_d is the argument of the minimization problem:

$$\underset{u_d}{\text{minimize}} \;\; J(u_d) = z(\text{diag}(u_d)u_d) \qquad \text{subject to} \;\; v_s - \Phi(u_d + \tilde{u}, \hat{\theta}_e) = 0,$$

where $\tilde{u} = u - u_d$, $J(u_d)$ is a cost function for minimizing the actuation effort (ergo, the power consumption), and z^T is a column vector of weighting constants. The Lagrangian function with Lagrangian parameter vector λ is introduced as

$$L(u_d, \tilde{u}, \lambda, \hat{\theta}_e, \hat{\theta}_u) = J(u_d) + (v_s - \Phi(u_d + \tilde{u}, \hat{\theta}_e))^T\lambda. \tag{23}$$

In [9], update laws for u_d, λ, $\hat{\theta}_e$ and $\hat{\theta}_u$ were developed to conserve the stability of the closed-loop system (1)-(2), (19) and (20). Two observers are used for the adaptive estimation of the uncertain parameters (θ_u and θ_e). With Hurwitz matrices ($-A_{\hat{u}}$) and ($-A_{\hat{x}}$), the two observers are

$$\dot{\hat{u}} = A_{\hat{u}}(u - \hat{u}) + f_{\theta_u}(u,u_{cmd})\hat{\theta}_u, \qquad \dot{\hat{x}} = A_{\hat{x}}(x - \hat{x}) + f(x) + g(x)\Phi(u,\hat{\theta}_e). \tag{24}$$

The four update laws for the adaptive control algorithm [9] are defined by

$$\begin{pmatrix}\dot{u}_d \\ \dot{\lambda}\end{pmatrix} = -\Gamma H \begin{pmatrix}\frac{\partial L}{\partial u_d} \\ \frac{\partial L}{\partial \lambda}\end{pmatrix} - u_{ff}, \qquad u_{ff} = H^{-1}\begin{pmatrix}\frac{\partial^2 L}{\partial\tilde{u}\partial u_d} \\ \frac{\partial^2 L}{\partial\tilde{u}\partial\lambda}\end{pmatrix} f_{\tilde{u}}(\tilde{u},u_d,u_{cmd},\hat{\theta}_u) + H^{-1}\begin{pmatrix}\frac{\partial^2 L}{\partial\hat{\theta}\partial u_d} \\ \frac{\partial^2 L}{\partial\hat{\theta}\partial\lambda}\end{pmatrix}\dot{\hat{\theta}},$$
$$\dot{\hat{\theta}}_e^T = \xi_x^T\Gamma_x g(x)\Phi_{\theta_e}(u)\Gamma_{\theta_e}^{-1}, \qquad H = \begin{pmatrix}\frac{\partial^2 L}{\partial u_d^2} & \frac{\partial^2 L}{\partial\lambda\partial u_d} \\ \frac{\partial^2 L}{\partial u_d\partial\lambda} & 0\end{pmatrix}, \tag{25}$$
$$\dot{\hat{\theta}}_u^T = \left(\frac{\partial V_{\tilde{u}}}{\partial\tilde{u}} + \xi_u^T\Gamma_u\right) f_{\theta_u}(u,u_{cmd})\Gamma_{\theta_u}^{-1} + \left(\xi_x^T\Gamma_x + \frac{\partial L^T}{\partial u_d}\frac{\partial^2 L}{\partial\tilde{u}\partial u_d} + \frac{\partial L^T}{\partial\lambda}\frac{\partial^2 L}{\partial\tilde{u}\partial\lambda}\right) f_{\theta_u}(u,u_{cmd})\Gamma_{\theta_u}^{-1},$$

where $\hat{\theta} \triangleq (\hat{\theta}_u^T, \hat{\theta}_e^T)^T$, $\xi_u \triangleq u - \hat{u}$, $\xi_x \triangleq x - \hat{x}$, and Γ, Γ_{θ_u}, Γ_{θ_e}, Γ_u and Γ_x are symmetric positive definite matrices.

Since the dynamics of all of the actuators take the same form (20), each actuator's low-level control law will have the same form. For brevity, only the low-level control law for $u_1 = P_{ic}$ is shown here. For the dynamic equation

$$\dot{u}_1 = \theta_{u,1}(u_{cmd,1} - u_1) \quad \longleftrightarrow \quad \dot{P}_{ic} = (1/\tau_{ic}^{lag})(P_{ic}^{cmd} - P_{ic}),$$

the Lyapunov function is chosen to be $V_{\tilde{u},1} = \tilde{u}_1^2/2$. Recalling (20), taking the time derivative of $V_{\tilde{u},1}$ and substituting the change in variables $\tilde{u}_1 = (u_1 - u_{d,1})$ gives

$$\dot{V}_{\tilde{u},1} = \tilde{u}_1\dot{\tilde{u}}_1 = \tilde{u}_1(\theta_{u,1}(u_{cmd,1} - \tilde{u}_1 - u_{d,1}) - \dot{u}_{d,1}).$$

When $\hat{\theta}_{u,1} = \theta_{u,1}$, the stability condition $\dot{V}_{\tilde{u},1} = -\tilde{u}_1^2\hat{\theta}_{u,1} < 0 \;\forall\; \tilde{u}_1 \neq 0$ is achieved (for $\theta_{u,1} > 0$) with the control law

$$u_{cmd,1} = u_{d,1} + \dot{u}_{d,1}/\hat{\theta}_{u,1}. \tag{26}$$

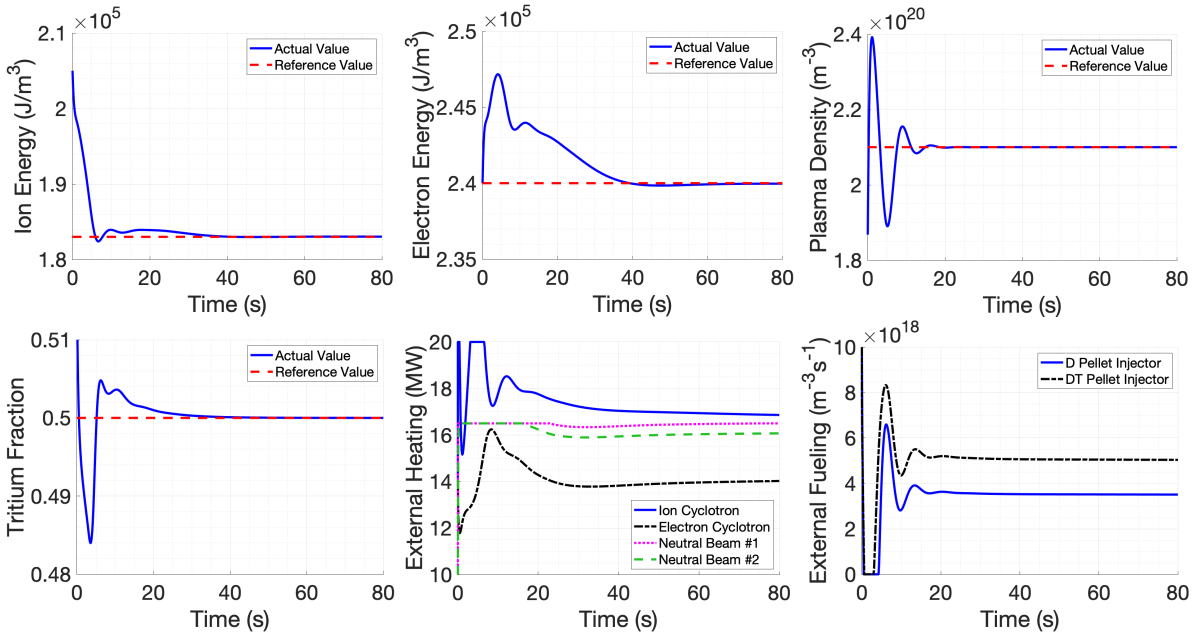

Figure 1: *Despite the model uncertainty and actuation lag, the burn control and control allocation algorithms successfully drive the plasma conditions to the desired reference values using ITER's various heating and fueling actuators. The first four plots show that the plasma's ion energy, electron energy, density and tritium fraction are brought to their reference values. The fifth and sixth plots show the commands for the ion cyclotron heating, the electron cyclotron heating, the neutral beam heating (from both injectors), the D pellet fueling, and the DT pellet fueling that are sent by the control allocator to the actuators before the actuator dynamics apply a lag to the actuation.*

The low-level control $u_{cmd,1}$ is manipulated in an attempt to force the actual actuator effort u_1, which is determined by the actuator dynamics (20), to the desired actuator effort $u_{d,1}$ that is calculated using (25). The Lyapunov functions and dynamics for each actuator is denoted $V_{\tilde{u},i}$ and $\dot{\tilde{u}}_i = f_{\tilde{u}_i}(\tilde{u}_i, u_{d,i}, u_{cmd,i}, \hat{\theta}_u)$ for $i \in \{1, ..., 6\}$. These are put into vectors $V_{\tilde{u}}$ and $f_{\tilde{u}}$ for use in (25). The remaining controls $u_{cmd,i}$ for $i \in \{2, ..., 6\}$ take the same form of (26).

7. Simulation Study

The following simulation study is an assessment of the presented adaptive burn control and control allocation algorithms. The simulation used $n_\alpha = 2.6 \times 10^{18}\text{m}^{-3}$, $n_D = 4.2 \times 10^{19}\text{m}^{-3}$, $n_T = 4.5 \times 10^{19}\text{m}^{-3}$, $n_I = 1 \times 10^{18}\text{m}^{-3}$, $E_i = 2.05 \times 10^5\text{J/m}^3$ and $E_e = 2.4 \times 10^5\text{J/m}^3$ as initial conditions ($Z_I = 4$). The uncertain parameters in the plasma model were set to $H = 1.1$, $\zeta_i = 1.15$, $\zeta_e = 0.85$, $\phi_\alpha = 0.15$, $k_D = 3$, $k_T = 2.5$, $k_\alpha = 6$, $k_I = 8.7$, $f_{eff} = 0.1$, $f_{ref} = 0.5$, $R^{eff} = 0.6$, $\gamma^{PFC} = 0.5$ and $f_I^{sp} = 0.01$. In the effector model, the uncertain parameters were set to $\eta_{ic} = 0.9$, $\eta_{ec} = 0.92$, $\eta_{nbi,1} = 1$, $\eta_{nbi,2} = 0.95$, $\eta_{Dpel} = 0.93$, $\eta_{DTpel} = 1$, $\gamma_{DTpel} = 0.9$ and $\phi_{nbi} = 0.25$. Respectively, the time constants τ_{ic}^{lag}, τ_{ec}^{lag}, τ_{nbi}^{lag} and τ_{pel}^{lag} were set to 5×0.2, 5×0.02, 5×0.58 and 5×0.1 seconds (a fivefold increase of the nominal plasma response times). The initial estimate of the uncertain vector $\hat{\Theta} \triangleq (\hat{\theta}_h^T, \hat{\theta}_e^T, \hat{\theta}_u^T)^T$ was calculated by multiplying the nominal values of each element, in order, with the following numbers: 1.09, 1.05, 0.95, 0.9, 0.92, 0.98, 1.07, 1.02, 1.10, 0.89, 0.91, 1.08, 1.16, 0.95, 0.89, 1.05, 1.11, 1.14, 0.89, 0.90, 0.95, 1.07, 1.18, 1.11 and 0.95. The upper saturation limits of ITERs actuators [7] are $P_{ic}^{max} = 20$ MW, $P_{ec}^{max} = 20$ MW, $P_{nbi,1}^{max} = 16.5$ MW, $P_{nbi,2}^{max} = 16.5$ MW, $S_{D_{pel}}^{max} = 120$ Pa m^3/s and $S_{DT_{pel}}^{max} = 111$ Pa m^3/s. The desired equilibrium point sent to the controller was chosen to be the solution of (9) with $d/dt = 0$ when $\bar{E}_i = 1.83 \times 10^5\text{J/m}^3$, $\bar{E}_e = 2.4 \times 10^5\text{J/m}^3$, $\bar{n} = 2.1 \times 10^{20}\text{m}^{-3}$ and $\bar{\gamma} = 0.5$.

Fig. 1 demonstrates the competence of the control and allocation algorithms in tracking target equilibria. Despite the uncertainty in the plasma confinement, wall recycling and ϕ_α, the adaptive burn controller successfully determines the four virtual control efforts ($P_{aux,i}$, $P_{aux,e}$, S_D, S_T) using (12)-(15) that will drive the system to the desired references. These virtual control efforts v_s are then sent to the adaptive control allocator which maps them to the six ITER actuators (P_{ic}, P_{ec}, $P_{nbi,1}$, $P_{nbi,2}$, $S_{D_{pel}}$, $S_{DT_{pel}}$). The control allocator successfully uses the six actuators to reproduce the four stabilizing virtual control efforts despite the uncertainty introduced in the effector model (19), the uncertainty in the actuator dynamics (20), and the nonzero actuation lag (T_{lag}). Fig. 1 shows the low-level control u_{cmd}, which is calculated using (26), that brings the actual (lagged) actuator efforts u, which are mapped back to the virtual control efforts v in (19), to the desired actuator effort u_d that is optimally calculated using the dynamic update laws (25).

8. Conclusions and Future Work

Actuation lag and the inclusion of uncertainty in the plasma model, effector model, and actuator dynamics make the plasma control problem more difficult. Together, the proposed adaptive burn controller and control allocator can overcome these challenges and force the nonlinear burning plasma system to desired equilibria. For future work, the effector model (19) can be expanded to consider DT gas puffing and impurity injection (from gas puffing and pellet injection). Since ITER's neutral beam injectors (NBI) will heat the plasma by firing highly kinetic deuterium particles into it, the fueling contribution from NBI can also be included in the effector model (for the deuterium fueling S_D specifically). Finally, future work may focus on modeling more specialized actuator dynamics for ITER. These new dynamics would then be considered in the formulation of a new optimal control allocation algorithm based on a possibly updated effector model.

Acknowledgments

Work supported by the U.S. Department of Energy, Office of Science, Office of Fusion Energy Sciences, under Award DE- SC0010661.

References

[1] J. Wesson, *Tokamaks*, Clarendon Press, Oxford, second edition (1997)

[2] M. Shimada et al., Physics Design of ITER-FEAT, J. Plasma Fusion Res., **3**, 77 (2000)

[3] V. Graber and E. Schuster, "Nonlinear Adaptive Burn Control of Two-Temperature Tokamak Plasmas", in *IEEE Conference Decision and Control*, Nice, France (2019)

[4] H. Khalil, *Nonlinear Systems*, Prentice Hall, New Jersey, third edition (2001)

[5] V. Graber and E. Schuster, "Nonlinear Adaptive Burn Control and Optimal Control Allocation of Over-Actuated Two-Temperature Plasmas", in *American Control Conference*, Denver, USA (2020)

[6] S. K. Combs, L. R. Baylor et al., Overview of recent developments in pellet injection for ITER, Fusion Eng. Des., **87** (2012)

[7] J. A. Snipes et al., Actuator and diagnostic requirements of the ITER Plasma Control System, Fusion Eng. and Design, **87** (2012)

[8] O. Harkegard and S. T. Glad, Resolving actuator redundancy - optimal control vs. control allocation, Automatica, **49**, 1087 (2013)

[9] J. Tjonnas and T. A. Johansen, "Optimizing adaptive control allocation with actuator dynamics", in *2007 46th IEEE Conference on Decision and Control*, 3780–3785 (2007)

[10] J. Ehrenberg, "Wall effects on particle recycling in tokamaks", in *Physical processes of the interaction of fusion plasmas with solids*, 35, Academic Press (1996)

[11] H. S. Bosch and G. M. Hale, Improved formulas for fusion cross-sections and thermal reactivities, Nucl. Fusion, **32** (1992)

[12] R. Gross, *Fusion Energy*, Wiley-Interscience, New York (1984)

[13] E. Doyle et al., Chapter 2: Plasma Confinement and Transport, Nucl. Fusion, **47** (2007)

[14] M. Shimada et al., Chapter 1: Overview and Summary, Nucl. Fusion, **47** (2007)

[15] D. Gallart, M. Mantsinen et al., "Modelling of ICRF Heating in DEMO with Special emphasis on Bulk Ion Heating", in *AIP Conference Proceedings*, volume 1689 (2015)

[16] R. S. Hemsworth et al., Overview of the design of the ITER heating neutral beam injectors, New J. Phys., **19** (2017)

[17] Krstić, Kanellakopoulos et al., *Nonlinear and Adaptive Control Design*, Wiley (1995)